Anal. Chem. **1998,** *70,* 2236−2242

Three-Dimensional Ion Mobility/TOFMS Analysis of Electrosprayed Biomolecules

Cherokee S. Hoaglund, Stephen J. Valentine, C. Ray Sporleder, James P. Reilly, and David E. Clemmer*

Department of Chemistry, Indiana University, Bloomington, Indiana 47405

An ion mobility/mass spectrometry technique has been developed to record mass-resolved ion mobility distributions for multiple ions simultaneously. The approach involves a new instrument that couples an electrospray ion source to an injected-ion drift tube/time-of-flight mass spectrometer. Individual components in a mixture of ions are separated by mobility differences in a drift tube and subsequently dispersed by mass-to-charge ratios in a time-of-flight instrument. Flight times in the mass spectrometer are much shorter than residence times in the drift tube, making it possible to record mass-resolved ion mobilities for all ions simultaneously. The result is a three-dimensional spectrum that contains collision cross section, mass-to-charge, and ion abundance information. The instrument and data acquisition system are described. Examples of combined ion mobility/time-of-flight data are presented for distributions of electrosprayed bradykinin and ubiquitin ions.

Ion mobility techniques[1,2] combined with mass spectrometry (MS) make it possible to distinguish between many types of ions that have identical mass-to-charge (m/z) ratios. A limitation of these methods is that mobilities and m/z ratios are measured independently. Ion mobility distributions are typically recorded for mass-selected ions by fixing a mass spectrometer to transmit only a narrow m/z window.[1,2] For systems where multiple ions are present, such as the charge state distributions formed by electrospray ionization (ESI),[3] separate ion mobility distributions must be recorded for each m/z ion. Recently, Guevremont et al. have reported essentially the reverse approach:[4] ions are selected by differences in their mobilities in a drift tube, and mass spectra are subsequently recorded using a time-of-flight (TOF) mass spectrometer. This requires that separate mass spectra be recorded for ions with different mobilities. In both the mass- and mobility-selected approaches, ions which are not selected are discarded during experiments. This introduces an inherent inefficiency in the method and precludes direct measurements of m/z- and conformer-resolved abundance information for the total ion system.

In this paper, we describe an injected-ion mobility/TOF mass spectrometer that is designed to record ion mobilities and m/z ratios for multiple ions simultaneously. Charge state distributions formed by ESI are separated by differences in their mobilities in a drift tube and then dispersed by their m/z ratios in the TOF instrument. This strategy makes it possible to record mass-resolved mobilities for all ions present in ESI distributions simultaneously. Thus, conformer- and m/z-resolved abundances for the total distribution of ions can be measured directly.

A number of recent studies have reported ion mobility distributions for biomolecular ions. Much of the recent interest in this approach is due to the fact that information about gas-phase conformations and the dynamics of folding and unfolding can be obtained.[2] Most work has involved peptides[5,6] or proteins,[2,7,8] and recently mobilities of oligosaccharides[9,10] and cross sections of DNA[11] have been reported. Several other ion mobility measurements have been made for biomolecules, with no attempt to extract information about conformations.[12−14]

(1) Ion mobility spectrometry methods are discussed in the following references: Hagen, D. F. *Anal. Chem.* **1979**, *51*, 870. Tou, J. C.; Boggs, G. U. *Anal. Chem.* **1976**, *48*, 1351. Karpas, Z.; Cohen, M. J.; Stimac, R. M.; Wernlund, R. F. *Int. J. Mass Spectrom. Ion Processes* **1986**, *83*, 163. St. Louis, R. H.; Hill, H. H. *Crit. Rev. Anal. Chem.* **1990**, *21*, 321. von Helden, G.; Hsu, M. T.; Kemper, P. R.; Bowers, M. T. *J. Chem. Phys.* **1991**, *95*, 3835. Jarrold, M. F. *J. Phys. Chem.* **1995**, *99*, 11.

(2) For recent reviews of ion mobility studies of biomolecules, see: Clemmer, D. E.; Jarrold, M. F. *J. Mass Spectrom.* **1997**, *32*, 577. Liu, Y.; Valentine, S. J.; Counterman, A. E.; Hoaglund, C. S.; Clemmer, D. E. *Anal. Chem.* **1997**, *69*, 728A.

(3) Fenn, J. B.; Mann, M.; Meng, C. K.; Wong, S. F.; Whitehouse, C. M. *Science* **1989**, *246*, 64.

(4) Guevremont, R.; Siu, K. W. M.; Wang, J.; Ding, L. *Anal. Chem.* **1997**, *69*, 3959.

(5) von Helden, G.; Wyttenbach, T.; Bowers, M. T. *Science* **1995**, *267*, 1483. Wyttenbach, T.; von Helden, G.; Bowers, M. T. *J. Am. Chem. Soc.* **1996**, *118*, 8355.

(6) Counterman, A. E.; Valentine, S. J.; Srebalus, C. A.; Henderson, S. C.; Hoaglund, C. S.; Clemmer, D. E. *J. Am. Soc. Mass Spectrom.*, in press.

(7) Clemmer, D. E.; Hudgins, R. R.; Jarrold, M. F. *J. Am. Chem. Soc.* **1995**, *117*, 10141. Shelimov, K. B.; Clemmer, D. E.; Hudgins, R. R.; Jarrold, M. F. *J. Am. Chem. Soc.* **1997**, *119*, 2240. Shelimov, K. B.; Jarrold, M. F. *J. Am. Chem. Soc.* **1997**, *119*, 2987. Woenckhaus, J.; Mao, Y.; Jarrold, M. F. *J. Phys. Chem. B* **1997**, *101*, 847. Woenckhaus, J.; Hudgins, R. R.; Jarrold, M. F. *J. Am. Chem. Soc.* **1997**, *119*, 9586.

(8) (a) Valentine, S. J.; Clemmer, D. E. *J. Am. Chem. Soc.* **1997**, *119*, 3558. (b) Valentine, S. J.; Anderson, J. G.; Ellington, A. D.; Clemmer, D. E. *J. Phys. Chem. B* **1997**, *101*, 3891. (c) Valentine, S. J.; Counterman, A. E.; Clemmer, D. E. *J. Am. Soc. Mass Spectrom.* **1997**, *8*, 954.

(9) Liu, Y.; Clemmer, D. E. *Anal. Chem.* **1997**, *69*, 2504.

(10) Lee, S.; Wyttenbach, T.; Bowers, M. T. *Int. J. Mass Spectrom. Ion Processes*, in press.

(11) Hoaglund, C. S.; Liu, Y.; Ellington, A. D.; Pagel, M.; Clemmer, D. E. *J. Am. Chem. Soc.* **1997**, *119*, 9051.

(12) Smith, R. D.; Loo, J. A.; Ogorzalek Loo, R. R.; Busman, M.; Udseth, H. R. *Mass Spectrom. Rev.* **1991**, *10*, 359. Smith, R. D.; Loo, J. A.; Ogorzalek Loo, R. R.; Udseth, H. R. *Mass Spectrom. Rev.* **1992**, *11*, 434.

(13) Wittmer, D.; Chen, Y. H.; Luckenbill, B. K.; Hill, H. H., Jr. *Anal. Chem.* **1994**, *66*, 2348. Chen, Y. H.; Hill, H. H., Jr; Wittmer, D. P. *Int. J. Mass Spectrom. Ion Processes* **1996**, *154*, 1.

S0003-2700(98)00059-6 CCC: $15.00
Published on Web 05/05/1998

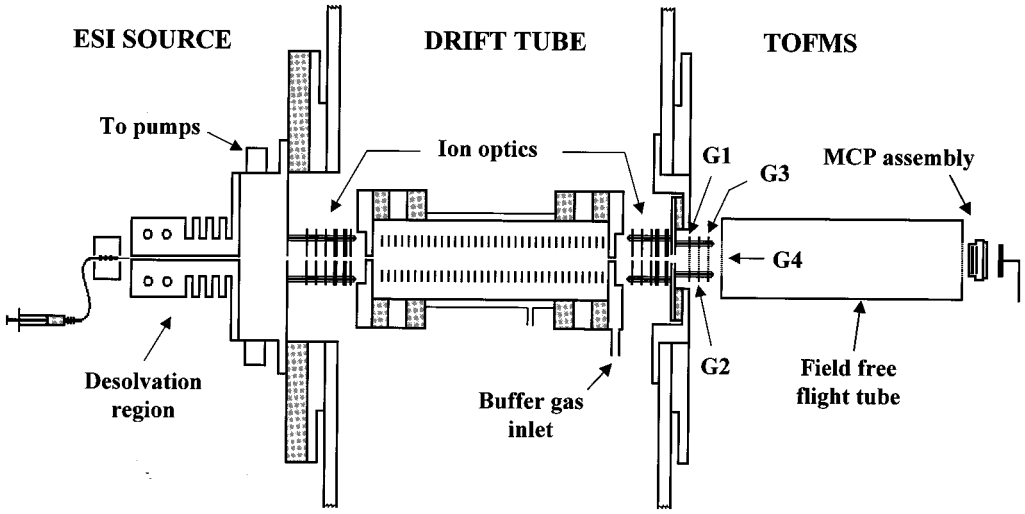

Figure 1. Schematic diagram of the experimental ion mobility/TOFMS instrument.

To illustrate the capability of measuring m/z-resolved mobilities for mixtures of ions, we have studied distributions of ubiquitin and bradykinin ions formed by ESI. Detailed ion mobility studies for these systems have been reported previously.[5,8c] The +6 to +13 charge states of ubiquitin exhibit an array of conformations, and the cross sections for these ions depend strongly on charge. A single elongated conformation type with cross sections ranging from 1650 to 1950 Å^2 was resolved for each of the +9 to +13 charge states. Ion mobility distributions for the +7 and +8 states are dominated by elongated conformations; smaller features corresponding to partially folded conformations are also present. A wide array of compact and partially folded conformers was observed for the +4 to +6 states.

Ion mobility studies of singly protonated bradykinin, formed by matrix-assisted laser desorption/ionization (MALDI),[15] have been carried out by Bowers and co-workers.[5] They report a cross section of 242 ± 5 Å^2 for the +1 state formed by MALDI and conclude that this ion has a tightly packed conformation, where the peptide folds around the charge.[5] Recently, we have measured cross sections of 239 ± 4 and 237 ± 4 Å^2 for singly and doubly protonated bradykinin ions (formed by ESI).[6] Within experimental uncertainties of 1−2%, our cross sections agree with the previous value. For the +1 ion (at m/z = 1061), we observed additional features in the ion mobility distributions that were attributed to formation of multiply protonated multimers. These results are discussed in more detail below.

In addition to ion mobility measurements, a number of other mass-spectrometry-based techniques provide information about the conformations of anhydrous biomolecules. These include isotopic hydrogen−deuterium exchange measurements,[8a,16] proton-transfer and ion molecule reactivity studies,[8c,17] dissociation and kinetic energy release measurements,[18] microscopy studies of high-energy surface impacts,[19] and ion scattering measurements of collision cross sections.[20] Several dissociation studies of bradykinin ions are also of related interest.[21,22]

EXPERIMENTAL SECTION

General. A schematic diagram of the injected-ion mobility/TOF mass spectrometer is shown in Figure 1. The instrument comprises four basic components: (1) an ESI source; (2) an injected-ion drift tube; (3) a TOF mass spectrometer; and (4) a data acquisition system. Each component is described in more detail below. A brief outline of a typical experimental sequence is as follows. Electrosprayed ions are extracted into a high-vacuum region (~10^{-5} Torr) and focused into an ion beam. Experiments are initiated by injecting a pulse of ions (50−100 μs in duration) into a drift tube containing He buffer gas. Ions drift through the gas under the influence of a weak, uniform electric field and are separated due to differences in their mobilities through the gas. When ions exit the drift tube, they are extracted

(14) Gieniec, J.; Mack, L. L.; Nakamae, K.; Gupta, C.; Kumar, V.; Dole, M.; *Biomed. Mass Spectrom.* **1984**, *11*, 259.
(15) Karas, M.; Hillenkamp, F. *Anal. Chem.* **1988**, *60*, 2299.
(16) Suckau, D.; Shi, Y.; Beu, S. C.; Senko, M. W.; Quinn, J. P.; Wampler, F. M., III; McLafferty, F. W. *Proc. Natl. Acad. Sci. U.S.A.* **1993**, *90*, 790. Wood, T. D.; Chorush, R. A.; Wampler, F. M., III; Little, D. P.; O'Connor, P. B.; McLafferty, F. W. *Proc. Natl. Acad. Sci. U.S.A.* **1995**, *92*, 2451. Winger, B. E.; Light-Wahl., J. J.; Rockwood, A. L.; Smith, R. D. *J. Am. Chem. Soc.* **1992**, *114*, 5897. Campbell, S.; Rodgers, M. T.; Marzluff, E. M.; Beauchamp, J. L. *J. Am. Chem. Soc.* **1995**, *117*, 12840. Gur, E. H.; de Koning, L. J.; Nibbering, N. M. M. *J. Am. Soc. Mass Spectrom.* **1995**, *6*, 466. Gard, E.; Green, M. K.; Bregar, J.; Lebrilla, C. B. *J. Am. Soc. Mass Spectrom.* **1994**, *5*, 623. Cassady, C. J.; Carr, S. R. *J. Mass Spectrom.* **1996**, *31*, 247. McLafferty, F. W.; Guan, Z.; Haupts, U.; Wood, T.; Kelleher, N. L. *J. Am. Chem. Soc.*, in press.
(17) (a) Ogorzalek Loo, R. R.; Smith, R. D. *J. Am. Soc. Mass Spectrom.* **1994**, *5*, 207. (b) Ogorzalek Loo, R. R.; Winger, B. E.; Smith, R. D. *J. Am. Soc. Mass Spectrom.* **1994**, *5*, 1064. (c) Schnier, P. F.; Gross, D. S.; Williams, E. R. *J. Am. Chem. Soc.* **1995**, *117*, 6747. (d) Gross, D. S.; Schnier, P. D.; Rodriguez-Cruz, S. E.; Fagerquist, C. K.; Williams, E. R. *Proc. Natl. Acad. Sci. U.S.A.* **1996**, *93*, 3143. (e) Williams, E. R. *J. Mass Spectrom.* **1996**, *31*, 831. (f) Cassady, C. J.; Wronka, J.; Kruppa, G. H.; Laukien, F. H. *Rapid Commun. Mass Spectrom.* **1994**, *8*, 394. (g) Zhang, X.; Cassady, C. J. *J. Am. Soc. Mass Spectrom.* **1996**, *7*, 1211. (h) McLuckey, S. A.; Stephenson, J. R., Jr. *Anal. Chem.* **1997**, *69*, 281.
(18) Kaltashov, I. A.; Fenselau, C. C. *J. Am. Chem. Soc.* **1995**, *117*, 9906. Adams, J.; Strobel, F.; Reiter, A. *J. Am. Soc. Mass Spectrom* **1996**, *7*, 30. Kaltashov, I. A.; Fenselau, C. C. *Proteins* **1997**, *27*, 165.
(19) Quist, A. P.; Ahlbom, J.; Reimann, C. T.; Sundquist, B. U. R. *Nucl. Instrum. Methods Phys. Res. B* **1994**, *88*, 164. Sullivan, P. A.; Axelsson, J.; Altmann, S.; Quist, A. P.; Sundquist, B. U. R.; Reinmann, C. T. *J. Am. Soc. Mass Spectrom.* **1996**, *7*, 329.
(20) Covey, T. R.; Douglas, D. J. *J. Am. Soc. Mass Spectrom.* **1996**, *4*, 616. Collings, B. A.; Douglas, D. J. *J. Am. Chem. Soc.* **1996**, *118*, 4488. Chen, Y.-L.; Collings, B. A.; Douglas, D. J. *J. Am. Soc. Mass. Spectrom.* **1997**, *8*, 681. Cox, K. A.; Julian, R. K.; Cooks, R. G.; Kaiser, R. E. *J. Am. Soc. Mass Spectrom.* **1994**, *5*, 127.
(21) Schnier, P. D.; Price, W. D.; Jockusch, R. A.; Williams, E. R. *J. Am. Chem. Soc.* **1996**, *118*, 7178.
(22) Heck, A. J. R.; Derrick, P. J. *Anal. Chem.* **1997**, *69*, 3603.

into a low-pressure chamber, pulsed into a flight tube for TOF mass analysis, and detected.

Ion Formation. Ubiquitin and bradykinin (Sigma 90% and 98% purity, respectively) were used for these studies. Positively charged (protonated) ions were formed by electrospraying solutions containing $10^{-4}-10^{-5}$ M protein (or peptide) solution in 49:49:2 (v/v/v) water/acetonitrile/acetic acid. The ESI needle was biased +3200 V relative to the entrance of the desolvation region. Typical solution flow rates are 0.10 mL/h. Solutions were electrosprayed at atmospheric pressures into a variable-temperature, differentially pumped desolvation region. This region is 5 cm long and is operated at a pressure of 1−10 Torr. Some of the ions exit the differentially pumped cavity through a 0.010-cm-diameter orifice and enter the main chamber of the instrument.

Injected-Ion Drift Tube. The present studies are carried out using an injected-ion drift tube that allows ions to be injected from high vacuum into the entrance of the high-pressure drift tube. The drift tube is 42.8 cm long, with 0.008-cm-diameter entrance and exit apertures. The body is made of concentric stainless steel tubes, allowing it to be heated or cooled by a hot fluid or liquid nitrogen, respectively. Entrance and exit plates are electrically isolated from the drift tube body with ceramic spacers machined from Mycalex (McMaster Carr). Thirty equally spaced 0.025-cm-thick BeCu rings are connected by a series of 5.00-MΩ high-vacuum resistors (KDI Electronics, ±1%) in order to create a uniform electric field along the drift axis. Data were recorded using ∼2−3 Torr of 300 K He buffer gas and applied drift fields of 3−15 V cm^{-1}.

As ions are injected into the drift tube, they are rapidly heated by initial collisions with the buffer gas, which thermalize their kinetic energies. Further collisions cool the ions to the temperature of the buffer gas. The injection voltage is defined by the voltage difference between the exit plate of the high-pressure source and the drift tube entrance plate. The injection energy is the injection voltage multiplied by the charge state of the ion. By varying the injection voltage, it is possible to induce conformational changes[2,7,8] as well as dissociation.[9] These changes can be monitored by measuring ion mobilities or mass spectra, providing information about folding and unfolding dynamics or fragmentation (sequence) information,[2,7,8,23] respectively.

Mass Spectrometer. When ions exit the drift tube, they are focused into the front of a simple linear TOF mass analyzer. The instrument is housed in a separate differentially pumped chamber, and typical pressures during experiments are $\sim 1 \times 10^{-6}$ Torr. Four entrance grids (labeled G1−G4 in Figure 1) are used to extract and pulse ions into the entrance of the flight tube. For the data shown below, grids were typically maintained near values of G1 = −60, G2 = −10, and G3 = +30 V. The G4 grid and flight tube are held at −8000 V. The potentials applied to G1 and G2 are sufficient to extract ions to the entrance of the flight tube, but the slightly positive potential applied to G3 prevents ions from being accelerated into the field-free region. A high-frequency (10^4 Hz), high-voltage (+500−+2000 V) pulser (Directed Energy Inc., model GRX-3.OK-H) is used to supply pulses (0.5−3 μs) to G2 in order to introduce ions into the region between G3 and G4. Here, they are accelerated to the flight tube potential and enter a 43.2-cm-long field-free region. Ions are detected by a pair of microchannel plates mounted directly to the back of the flight tube.

Ion Mobility and TOF Considerations. For this discussion, the term *drift time* is defined as the time required for ions to travel through the high-pressure drift tube, as given by[24]

$$t_D = L/E_D K \tag{1}$$

where K is the mobility of the ions, L is the length of the drift tube, and E_D is the applied drift field. The term *flight time* refers to the time required for ions that have been accelerated to a desired kinetic energy in a vacuum to travel through the field-free region of the mass spectrometer. The flight time is

$$t_F = l(m/2zE_{TOF})^{1/2} \tag{2}$$

where l is the length of the field-free region, m is the ion mass, z is the ion charge state, and E_{TOF} is the kinetic energy of the ions.

The arrival time of a packet of ions at the detector is a composite of the drift time, flight time, and the time required to travel through other portions of the instrument. Thus, it is necessary to account for the flight time and a small correction associated with transport of the ions from the exit of the drift tube to the entrance of the time-of-flight region in determining t_D. The correction time is small (80−140 μs) compared to the 2−5-ms drift times in these experiments.

Collision cross sections are derived directly from experimental drift times using the expression[2,24,25]

$$\Omega = \frac{(18\pi)^{1/2}}{16}\frac{ze}{(k_B T)^{1/2}}\left[\frac{1}{m_I}+\frac{1}{m_B}\right]^{1/2}\frac{t_D E}{L}\frac{760}{P}\frac{T}{273.2}\frac{1}{N} \tag{3}$$

where N is the neutral number density, k_B is the Boltzmann constant, and m_I and m_B are the masses of the ion and buffer gas, respectively. All of the parameters E_D, L, P, T, and t_D can be precisely measured. Thus, the reproducibility of measured cross sections is excellent. Ion energies in the drift tube are determined by E_D/N. The present experiments were carried out at low E_D/N, where mobilities are independent of the applied drift field, and drift velocities are small compared with the thermal velocity of the buffer gas. Under these conditions, ions are not expected to align in the drift tube, and we assume that collision cross sections correspond to an average of all possible orientations.

Acquisition of Nested Drift (Flight) Time Data. Simultaneous measurements of drift times and flight times are feasible because flight times are much shorter than drift times. Thus, flight time measurements of the different m/z ions can be nested within individual time windows of the ion mobility spectrum. Figure 2 shows the pulse sequence for injection of the initial pulse of ions into the drift tube followed by time-of-flight analysis. Ions are injected into the drift tube at repetition rates of 10−30 Hz and into the flight tube at 10^4 Hz. With a time-of-flight mass analyzer, it is possible to observe all m/z species that are present

(23) Jarrold, M. F.; Honea, E. C. *J. Phys. Chem.* **1991**, *95*, 9181. Jarrold, M. F.; Constant, V. A. *Phys. Rev. Lett.* **1991**, *67*, 2994.

(24) Mason, E. A.; McDaniel, E. W. *Transport Properties of Ions in Gases*; Wiley: New York, 1988.

(25) Hirschfelder, J. O.; Curtiss, C. R.; Bird, R. B. *Molecular Theory of Gases and Liquids*; Wiley: New York, 1964 (c1954).

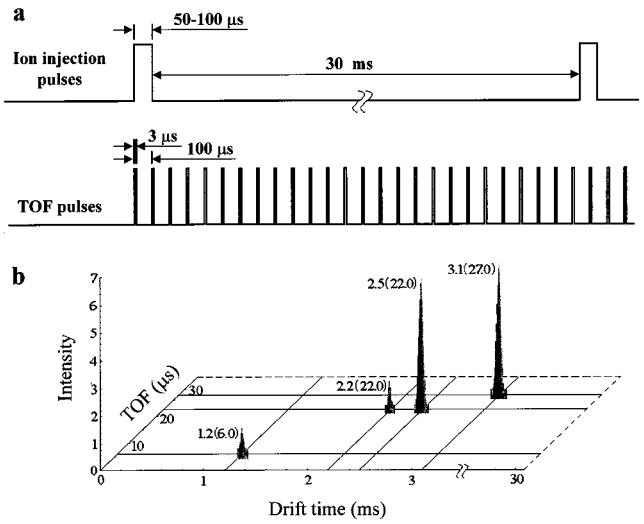

Figure 2. (a) Pulse sequence employed to record an example nested $t_D(t_F)$ spectrum for multiple ions. (b) Example spectrum which consists of mass- and mobility-resolved distributions for multiple ions. Peaks in this distribution are separated by differences in their mobilities in the drift tube and then dispersed according to their m/z ratios in the TOF instrument.

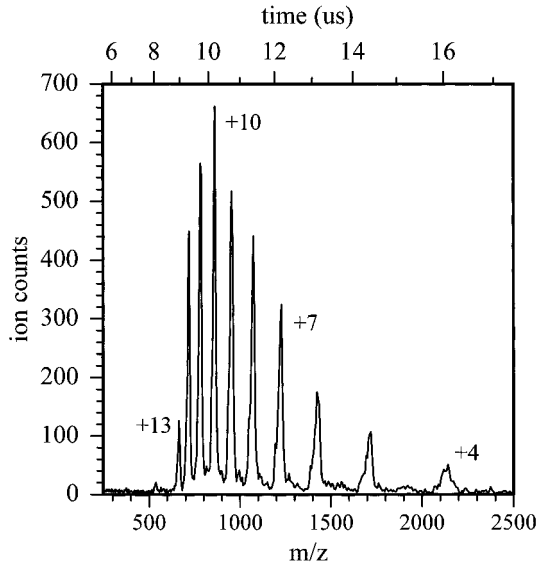

Figure 3. Mass spectrum recorded for electrosprayed ubiquitin ions in the linear TOF instrument. In this spectrum, the initial injection pulse has been disabled, allowing ions to be continuously injected into the drift tube at a nominal injection voltage of 80 V. Ions were extracted into the entrance region using grid voltages of G1 = −66, G2 = −9, G3 = +33, and G4 = −8000 V. A +1737-V pulse, 2.0 μs in duration at 10 kHz, was used to initiate the TOF experiment.

in each drift time window. Thus, mass-resolved ion mobility distributions are simultaneously recorded for all m/z species.

We denote the nested drift and flight times by giving the drift time followed by the flight time in parentheses, $t_D(t_F)$. In the present data, drift times and flight times are given in units of milliseconds and microseconds, respectively. Figure 2b shows an example spectrum. Here, the first ions to exit the drift tube are observed at 1.2(6.0), and the last ions to exit are observed at 3.1(27.0). Peaks at 2.2(22.0) and 2.5(22.0) have identical flight times but different drift times. This type of behavior is observed for different conformations or isomers with the same m/z ratios but different mobilities.

Acquisition of $t_D(t_F)$ distributions is carried out as follows. The initial injection pulse activates a programmable delay generator (PDG, Lecroy 4222) that triggers the high-voltage TOF pulser at specified delay times. In these experiments, an accumulation of 256 windows (each 100 μs in duration) creates the ion mobility distribution. Flight times in the mass spectrometer are recorded using a time-to-digital converter (TDC, Lecroy 4208) that is also initiated by the PDG pulse sequence. The TDC records the time that ions reach the detector during the first 32 μs of the 100-μs drift time window, with 1-ns resolution. Up to eight events for each TOF pulse (or drift time window) can be recorded by the TDC. Only times associated with ions striking the detector are transferred to the computer, facilitating the readout and storage of the TOF data. The instrumental electronics and data acquisition system, including the initial injection pulse, PDG pulse sequence, TDC, and high-voltage TOF pulser, are synchronized by an interface and controlled by a Pentium computer.

It is often necessary to delay activation of the TDC (usually 0.5−2 μs) in order to avoid saturation due to noise events associated with each high-voltage pulse. Data files are a compilation of drift and flight times of every ion that hits the detector and are usually too large to be stored on floppy disks. Thus, the acquisition computer is linked to an NT Pentium Pro server, and data are downloaded for analysis. Peak identification and integration programs were written in-house. Three-dimensional plots of the data shown were created using the Insight II molecular modeling software.[26]

RESULTS AND DISCUSSION

Time-of-Flight Mass Spectra. Time-of-flight mass spectra (without mobility-based separation) can be recorded for the continuous beam of electrosprayed ions by disabling the initial injection pulse. Under these conditions, ions continuously exit the drift tube, are focused into the entrance of the TOF instrument, and are pulsed into the flight tube at a repetition rate of 10 kHz. An example time-of-flight spectrum measured for an ESI charge state distribution of ubiquitin is shown in Figure 3. The peaks observed are characteristic of those expected for the +4 to +13 protonation states. Previous ESI mass spectra reported for ubiquitin are similar.[8c,17a,b,f,g]

Nested $t_D(t_F)$ Measurements of Ubiquitin. Figure 4 shows mass-resolved ion mobility data for a distribution of electrosprayed ubiquitin ions that were injected into the drift tube at 80 V. Note that time of flight increases from right to left in Figure 4. This perspective conveys the most information about the three-dimensional data. The peaks in Figure 4 have the same flight times as the peaks in the time-of-flight mass spectrum shown in Figure 3; thus, m/z ratios are assigned as above. Drift and flight times for the +7 to +13 ions increase systematically with increasing m/z: 4.11(12.2) for +7, 3.79(11.4) for +8, 3.48(10.7) for +9, 3.28-(10.2) for +10, 3.10(9.7) for +11, 3.01(9.3) for +12, and 2.90(9.0) for +13. This behavior is expected for a series of ions with the same mass and similar collision cross sections. The distribution of drift times observed for the +7 ion shows a sharp peak at 4.1 ms and a tail associated with higher mobility ions that extends to

(26) Insight II; BIOSYM/MSI: San Diego, CA, 1995.

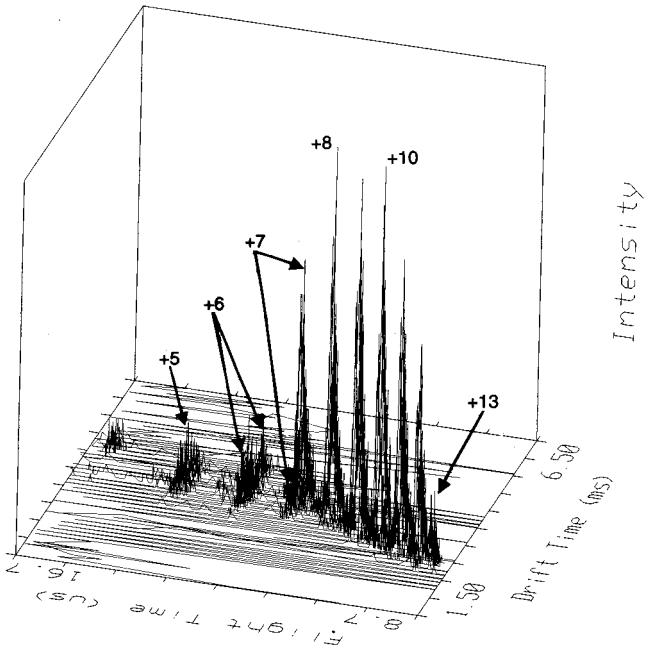

Figure 4. Three-dimensional representation of drift time, flight time, and ion abundances for a distribution of electrosprayed ubiquitin ions. These data were obtained upon enabling the initial injection pulse under the same experimental conditions as in Figure 3. The drift tube was operated using a drift field of 14.53 V cm^{-1}, under 2.059 ± 0.006 Torr of He buffer gas. This spectrum was recorded using an injection voltage of 80 V.

3.6 ms. These drift times are similar to data reported previously for the +7 ion and indicate that a small distribution of partially folded conformations is present.[8c] A broad range of drift times (3.5−4.5 ms) is observed for the +5 and +6 charge states, indicating that multiple conformations are present. The +4 ion is observed over a narrower range (4.4−4.7 ms).

Collision cross sections derived from these data range from 980 to 1941 Å^2 for the most compact +4 ion to the most elongated +13 state. This range of values is in excellent agreement with the range of 980−1912 Å^2 that we reported previously for these ions.[8c] Individual drift times for sharp features, such as the elongated conformations observed for the +7 to +13 charge states, typically agree to within 1−3% of values derived previously. The agreement of these data with those recorded by the selected-ion method demonstrates that cross sections for an array of ions can be measured simultaneously with the nested data acquisition approach.

Direct information about the abundance of each conformation within each charge state can be obtained by a two-dimensional integration of the peak. Previously, we divided the collision cross sections recorded for ubiquitin into three conformation types: compact conformations, defined as those features in the ion mobility distributions having cross sections below 1120 Å^2 (+4 to +6 ions); elongated conformations, for ions with cross sections greater than 1500 Å^2 (+6 to +13 ions at high injection energies); and conformations that were referred to as partially folded, that had cross sections between these values (+5 to +8 ions). Integration of the data with respect to these assignments shows that the distribution of ions is comprised of 77% elongated conformers (found for the +7 to +13 ions); 15% partially folded conformers (in the +6 and +7 states); and 7% compact conformers (in the +4 to +6 states). Absolute conformer abundances within individual charge states are given in Table 1.

Table 1. Mobility-Resolved Ion Abundances for Electrosprayed Ubiquitin Ions[a]

m/z[b]	charge state assignment	compact[c]	partially folded[d]	elongated[e]
2140	+4	2.2	0.0	0.0
1715	+5	2.3	5.1	0.0
1427	+6	2.7	5.1	3.3
1226	+7	0.0	2.9	12.7
1074	+8	0.0	2.3	12.1
956	+9	0.0	0.0	14.6
861	+10	0.0	0.0	13.2
785	+11	0.0	0.0	11.6
720	+12	0.0	0.0	7.6
664	+13	0.0	0.0	2.3

[a] Abundances were derived by integration of peak areas over defined drift time and flight time ranges. [b] m/z ratios are determined from calibrated flight times as described in text. [c] Abundances obtained by integrating over a range of drift times which corresponds to compact-conformations with cross sections that are less than 1120 Å^2. [d] Abundances obtained by integrating over a range of drift times which corresponds to partially folded conformations (1120 < Ω < 1500 Å^2). [e] Abundances obtained by integrating over a range of drift times which corresponds to elongated conformations (Ω ≥ 1500 Å^2).

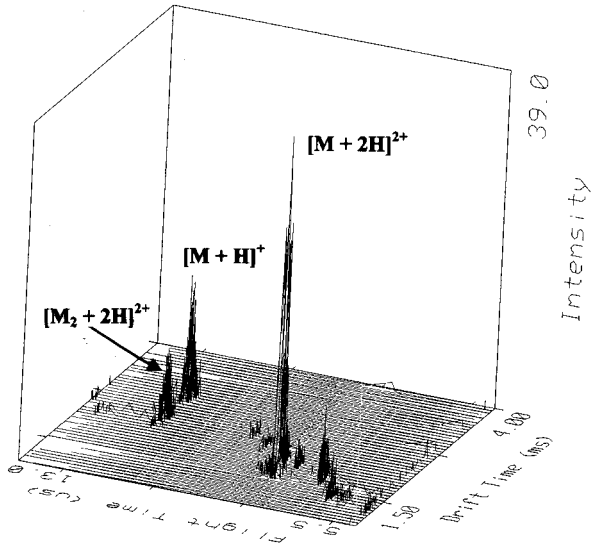

Figure 5. Three-dimensional representation of drift time, flight time, and ion abundances for a distribution of electrosprayed bradykinin ions that have been injected into the drift tube using 80 V. The dominant peaks in this spectrum are assigned to a doubly charged monomer ([M + 2H]$^{2+}$ having drift and flight times of 2.2 ms and 8.0 μs, respectively), a singly charged monomer ([M + H]$^+$ having drift and flight times of 4.2 ms and 11.3 μs), and a doubly charged dimer ([M$_2$ + 2H]$^{2+}$ having drift and flight times of 3.4 ms and 11.3 μs). See the text for a detailed discussion of these assignments.

Bradykinin. Figure 5 shows nested $t_D(t_F)$ distributions for electrosprayed bradykinin ions that have been injected into the drift tube at 80 V. The spectrum is dominated by a sharp peak at 2.2(8.0) that we assign to the +2 charge state (m/z = 531) of bradykinin. Both 4.2(11.3) and 3.4(11.3) peaks corresponds to m/z = 1061 (the nominal +1 state of bradykinin). A series of much smaller peaks, with $t_D(t_F)$ values ranging from 1.83(6.3) to 3.38(9.3), is also observed.

To assign the two peaks for the m/z = 1061, we note that a cross section of 245 Å^2 corresponds to a tightly packed, roughly

Table 2. Mobility-Resolved Ion Abundances for Electrosprayed Bradykinin Ions[a]

$t_D(t_F)$[b]	assignment	abundance (%) 80 V	140 V
2.24(8.0)	$[M + 2H]^{2+}$	42.0	19.0
4.21(11.3)	$[M + H]^{+}$	21.1	55.0
3.38(11.3)	$[M_2 + 2H]^{2+}$	11.5	2.0
1.83(6.3)	$m/z = 328$	2.3	
1.83(6.6)	$m/z = 360$	4.4	
2.65(7.0)	$m/z = 406$	8.2	2.7
2.65(7.9)	$m/z = 517$	2.6	
2.76(8.2)	$m/z = 557$	4.4	2.0
3.17(8.8)	$m/z = 641$	2.1	1.0
3.38(9.3)	$m/z = 716$	1.5	3.0
3.59(9.9)	$m/z = 811$		6.4
3.79(10.2)	$m/z = 861$		6.0
4.21(11.5)	$m/z = 1095$		3.0

[a] Abundances are obtained by a two-dimensional integration of drift and flight times over specified ranges. [b] Drift times t_D and flight times t_F are given in milliseconds and microseconds, respectively. The $t_D(t_F)$ nomenclature is discussed in the text.

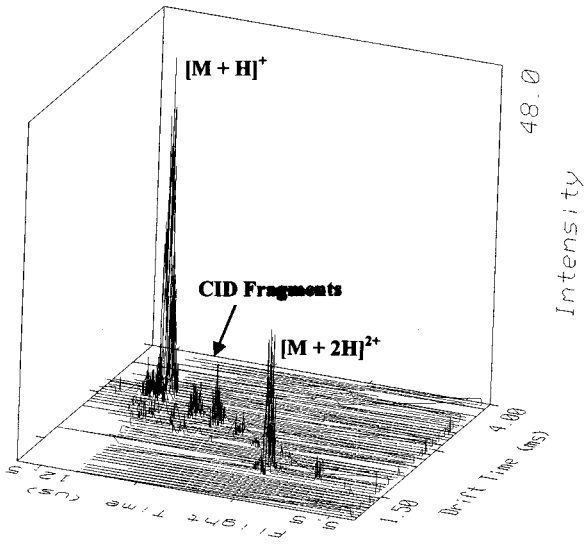

Figure 6. Three-dimensional representation of drift time, flight time, and ion abundances for a distribution of electrosprayed bradykinin ions that have been injected into the drift tube at 140 V. Peaks are assigned as discussed in the caption for Figure 5.

spherical form. From the data in Figure 5, we derive a cross section of 239 Å^2 for the peak at 4.2(11.3). This value agrees with the 245-Å^2 value measured previously, within the combined uncertainty of both measurements. Thus, we assign this peak to singly protonated bradykinin monomer, $[M + H]^+$. The ions at 3.4(11.3) have mobilities that are ~20% higher, and attempts to assign them as more compact $[M + H]^+$ forms using molecular modeling methods[26] have failed. As mentioned above, other studies in our laboratory provide convincing evidence that this peak is due to a doubly protonated dimer, $[M_2 + 2H]^{2+}$, form of bradykinin.[6] This doubly protonated ion has a slightly shorter drift time than the compact monomer. This can be understood by considering that, although the cross section of the dimer is larger than the monomer, the doubly charged dimer experiences a larger effective drift field, and the surface area per monomer unit decreases when the monomers associate. The composition of the ion distribution is obtained by integration of peak areas and is given in Table 2. The major $[M + 2H]^{2+}$, $[M + H]^+$, and $[M_2 + 2H]^{2+}$ ions have relative abundances of 42, 21, and 12%, respectively. Smaller features observed in this distribution comprise the remaining 26% of the distribution.

When ions are injected into the drift tube at high injection voltages, the ion distribution changes dramatically, as shown in Figure 6 for data recorded at 140 V. Here, the $[M + H]^+$ peak comprises 55% of the total fraction of ions. The peak at 3.4(11.3) for $[M_2 + 2H]^{2+}$ is substantially depleted, accounting for only ~2% of the total ion abundance. The decrease in intensity (from 11.5% at 80 V to 2% at 140 V) can be explained by noting that, at high injection voltages, this ion can dissociate to form two $[M + H]^+$ monomers. The corresponding 34% increase in the $[M + H]^+$ abundance (from 21 to 55%, Table 1) is slightly higher than the 23% increase expected from dissociation of $[M_2 + 2H]^{2+}$ dimer; thus, the relative abundances of other ions must also change as a function of injection voltage.

The $[M + 2H]^{2+}$ ion is also apparent in Figure 6; however, the relative abundance of this ion (19%) is much less than the 42% abundance in Figure 5. This ion could be depleted by collision-induced dissociation or endothermic proton transfer with the buffer gas during the injection process. Several peaks at 10.2, 9.9, and 9.3 μs that correspond to m/z ratios of 860, 810, and 710 are consistent with dissociation products (at 858.5, 807.4, and 710.4) of this ion measured recently by collisional activation in an FTICR.[22,27] It is possible that this 15.4% population comes from dissociation of $[M + 2H]^{2+}$. However, this fraction is too small to account for the 23% depletion of $[M + 2H]^{2+}$ observed. Endothermic proton transfer would form the $[M + H]^+$ monomer; this may account for the observation that the abundance of this ion is 14% higher than could be accounted for by dissociation of the $[M_2 + 2H]^+$ dimer alone.

Comparison to Selected-Ion Measurements. Compared with selected-ion methods, nested $t_D(t_F)$ measurements offer a number of important advantages. For example, the data collection process is simplified. Selected-m/z methods require that independent ion mobility distributions be measured for each ion that is observed in the mass spectrum. Similarly, the mobility-selected approach requires that separate mass spectra be recorded for each range of selected mobilities. As shown above, nested $t_D(t_F)$ measurements record m/z-selected ion mobility distributions for all ions simultaneously. This yields a single spectrum that contains m/z, mobility, and ion abundance information for all species that are present. Direct measurements of conformer-resolved ion abundances for entire ion distributions are extremely useful in discerning the origins of different conformations and charge states during injection into the drift tube. Similarly, studies at low injection energies will provide insight into the origin of ions during the electrospray process. Finally, although it was not emphasized above, the combined methods lead to a net improvement in the ability to resolve peaks (compared to the individual mobility separation or time-of-flight instruments we have used).

(27) It is noteworthy that we did not observe fragments at $m/z = 904.5$ and 886.5, as these are the largest peaks observed upon collisional activation in an FTICR. Differences in biomolecular collision-induced dissociation pathways in a high-pressure drift tube and those observed in low-pressure instruments have been observed previously (ref 9).

Although this work demonstrates that nested $t_D(t_F)$ measurements are feasible, it is important to note that this method has not been optimized. The overall experimental duty cycle used to record the data in Figures 4−6 was extremely low. More than 99% of the ion signal was discarded during the initial injection pulse. We have recently shown that an ion trap interface for the continuous ESI source can improve signal-to-noise ratios by factors of 10−30.[28] Further inefficiencies are associated with the time-of-flight pulse sequence (Figure 2); at least 3 times more ions than were used in these studies are available. The most dramatic improvements that remain are associated with the resolving powers of the drift tube and time-of-flight instruments. Clearly, these improvements will lead to better separation and identification of ions. Additionally, signal-to-noise ratios increase proportionally with resolution as ion signals are compressed into fewer $t_D(t_F)$ bins. This is a unique advantage of time-of-flight methods over mass filters.

SUMMARY AND CONCLUSIONS

An ion mobility/mass spectrometry technique that allows nested $t_D(t_F)$ measurements to be obtained has been described. These methods make it possible to obtain mass-resolved ion mobility distributions for a distribution of ions simultaneously. The approach involves an instrument that couples an injected-ion drift tube with a linear time-of-flight mass spectrometer. The ability to measure m/z-resolved ion mobility distributions for multiple ions simultaneously has a number of distinct advantages, including

(1) improved efficiency in recording collision cross sections for many different species in the distribution of ions system,

(2) a net improvement in the ability to resolve different peaks (compared to the individual mobility separation or m/z dispersion), and

(3) direct measurements of conformer and m/z abundances for the ion distribution.

Further improvements in the overall experimental duty cycle and resolving powers of the ion mobility and time-of-flight mass spectrometer will provide greater signal-to-noise ratios for these experiments. Efforts in our laboratory to develop a high-resolution drift tube and off-axis and reflectron time-of-flight instruments for nested $t_D(t_F)$ measurements are currently underway.

ACKNOWLEDGMENT

We acknowledge many insightful comments regarding display and analysis of these data by Anne E. Counterman. This work was supported by grants from the NSF (CHE-9625199) and NIH (1R01GM55647-02) and an ASMS Research Award from Finnegan MAT.

Received for review January 22, 1998. Accepted March 31, 1998.

AC980059C

(28) Hoaglund, C. S.; Valentine, S. J.; Clemmer, D. E. *Anal. Chem.* **1997**, *69*, 4156.